



Mid-infrared Vernier racetrack resonator tunable filter implemented on a germanium on SOI waveguide platform [Invited]

SANJA RADOSAVLJEVIC,* NURIA TEIGELL BENEITEZ, ANDREW KATUMBA, MUHAMMAD MUNEEB, MICHAEL VANSLEMBROUCK, BART KUYKEN, AND GUNTHER ROELKENS

Photonics Research Group, Ghent University - imec, Technologiepark 15, 9052 Ghent, Belgium
Center for Nano- and Biophotonics, Technologiepark 15, 9052 Ghent, Belgium

*sanja.radosavljevic@ugent.be

Abstract: Currently, most widely tunable lasers rely on an external diffraction grating to tune the laser wavelength. In this paper we present the realization of a chip-scale Vernier tunable racetrack resonator filter on the Ge-on-SOI waveguide platform that allows for wide tuning (108 nm free spectral range) in the 5 μm wavelength range without any moving parts. The fabricated racetrack resonators have a loaded Q-factor of 20000, resulting in a side-peak suppression of more than 20 dB, which is more than sufficient for wavelength selection in an external cavity laser.

© 2018 Optical Society of America under the terms of the [OSA Open Access Publishing Agreement](#)

OCIS codes: (130.7408) Wavelength filtering devices; (130.3120) Integrated optics devices; (130.3060) Infrared.

References and links

1. M. Yu, Y. Okawachi, A. G. Griffith, N. Picqué, M. Lipson, and A. L. Gaeta, "Silicon-chip-based mid-infrared dual-comb spectroscopy," arXiv preprint arXiv:1610.01121 (2016).
2. L. Tombez, E. J. Zhang, J. S. Orcutt, S. Kamlapurkar, and W. M. J. Green, "Methane absorption spectroscopy on a silicon photonic chip," *Optica*, **4**(11), 1322-1325 (2017).
3. P.A. Werle, "Review of recent advances in semiconductor laser based gas monitors," *Spectrochim. Acta Mol. Biomol. Spectrosc.* **54**(2), 197-236 (1998).
4. J. Hodgkinson and R.P. Tatam, "Optical gas sensing : a review," *Meas. Sci. Technol.* **24**(1), 012004 (2012).
5. M. Nedeljkovic, A.V. Velasco, A.Z. Khokhar, A. Delège, P. Cheben, and G.Z. Mashanovich, "Mid-infrared silicon-on-insulator Fourier-transform spectrometer chip," *IEEE Photon. Technol. Lett.* **28**(4), 528-531 (2016).
6. F. Adler, P. Masłowski, A. Foltynowicz, K.C. Cossel, T.C. Briles, I. Hartl, and J. Ye, "Mid-infrared Fourier transform spectroscopy with a broadband frequency comb," *Opt. Express* **18**(21), 21861-21872 (2010).
7. R.A. Soref, "Mid-infrared photonics in silicon and germanium," *Nat. Photon* **4**(8), 495-497 (2010).
8. M. Muneeb, X. Chen, P. Verheyen, G. Lepage, S. Pathak, E.M.P. Ryckeboer, A. Malik, B. Kuyken, M. Nedeljkovic, J. Van Campenhout, G. Mashanovich, and G. Roelkens, "Demonstration of silicon on insulator midinfrared spectrometers operating at 3.8 μm ," *Opt. Express* **21**(10), 11659-11669 (2013).
9. Z. Cheng, X. Chen, C.Y. Wong, K. Xu, and H.K. Tsang, "Mid-infrared suspended membrane waveguide and ring resonator on silicon-on-insulator," *IEEE Photon. J.* **4**(5), 1510-1519 (2012).
10. T. Baehr-Jones, A. Spott, R. Ilic, A. Spott, B. Penkov, W. Asher, and M. Hochberg, "Silicon-on-sapphire integrated waveguides for the mid-infrared," *Opt. Express*, **18**(12), 12127-12135 (2010).
11. J.M. Ramirez, V. Vakarin, C. Gilles, J. Frigerio, A. Ballabio, P. Chaisakul, X. Le Roux, C. Alonso-Ramos, G. Maisons, L. Vivien, M. Carras, G. Isella, and D. Marris-Morini, "Low-loss Ge-rich $\text{Si}_{0.2}\text{Ge}_{0.8}$ waveguides for mid-infrared photonics," *Opt. Lett.* **42**(1), 105-108 (2017).
12. A. Malik, M. Muneeb, S. Pathak, Y. Shimura, J. Van Campenhout, R. Loo, and G. Roelkens, "Germanium-on-silicon mid-infrared arrayed waveguide grating multiplexers," *IEEE Photon. Technol. Lett.* **25**(18), 1805-1808 (2013).
13. A. Malik, M. Muneeb, Y. Shimura, J. Van Campenhout, R. Loo, and G. Roelkens, "Germanium-on-silicon planar concave grating wavelength (de)multiplexers in the mid-infrared," *Appl. Phys. Lett.* **103**(16), 161119 (2013).
14. G. Z. Mashanovich, C. J. Mitchell, J. S. Penades, A. Z. Khokhar, C. G. Littlejohns, W. Cao, Z. Qu, S. Stanković, F. Y. Gardes, T. Ben Masaud, H. M. H. Chong, V. Mittal, G. Senthil Murugan, J. S. Wilkinson, A. C. Peacock, and M. Nedeljkovic, "Germanium mid-infrared photonic devices," *Journal of Lightwave Technology* **35**(4), 624-630 (2017).
15. B. Troia, J. S. Penades, A. Z. Khokhar, M. Nedeljkovic, C. Alonso-Ramos, V. M. Passaro, and G. Z. Mashanovich, "Germanium-on-silicon Vernier-effect photonic microcavities for the mid-infrared," *Opt. Lett.* **41**(3), 610-613 (2016).
16. A. Malik, S. Dwivedi, L. Van Landschoot, M. Muneeb, Y. Shimura, G. Lepage, J. Van Campenhout, W. Vanherle, T. Van Opstal, R. Loo, and G. Roelkens, "Ge-on-Si and Ge-on-SOI thermo-optic phase shifters for the mid-infrared," *Opt. Express* **22**(23), 28479-28488 (2014).

17. S. Radosavljevic, B. Kuyken, and G. Roelkens, "Efficient 5.2 μm wavelength fiber-to-chip grating couplers for the Ge-on-Si and Ge-on-SOI mid-infrared waveguide platform." *Opt. Express* **25**(16), 19034–19042 (2017).
18. M. Razeghi, Q. Y. Lu, N. Bandyopadhyay, W. Zhou, D. Heydari, Y. Bai, and S. Slivken, "Quantum cascade lasers: from tool to product." *Opt. Express* **23**(7), 8462–8475 (2015).
19. I. Vurgaftman, C. L. Canedy, C. S. Kim, M. Kim, W. W. Bewley, J. R. Lindle, J. Abell, and J. R. Meyer, "Mid-infrared interband cascade lasers operating at ambient temperatures," *New Journal of Physics* **11**(12), 125015 (2009).
20. Q. Y. Lu, Y. Bai, N. Bandyopadhyay, S. Slivken, and M. Razeghi, "Room-temperature continuous wave operation of distributed feedback quantum cascade lasers with watt-level power output," *App. Phys. Lett.* **97**(23), 231119 (2010).
21. I. Vurgaftman, W. W. Bewley, C. L. Canedy, C. S. Kim, M. Kim, C. D. Merritt, J. Abell, J. R. Lindle, and J. R. Meyer, "Rebalancing of internally generated carriers for mid-infrared interband cascade lasers with very low power consumption," *Nature Communications* **2**, 585 (2011).
22. Q. Yang, F. Fuchs, and J. Wagner, "Quantum cascade lasers (QCL) for active hyperspectral imaging," *Advanced Optical Technologies* **3**(2), 141–150 (2014).
23. http://www.spectralcalc.com/spectral_browser/db_intensity.php
24. W. Bogaerts, P. De Heyn, T. Van Vaerenbergh, K. De Vos, S. Kumar Selvaraja, T. Claes, P. Dumon, P. Bienstman, D. Van Thourhout, and R. Baets, "Silicon microring resonators," *Laser Photonics Reviews*, **6**(1), 47–73 (2012).
25. https://www.thorlabs.com/newgrouppage9.cfm?objectgroup_id=7062
26. B. J. Frey, D. B. Leviton, and T. J. Madison, "Temperature dependent refractive index of silicon and germanium," arXiv preprint physics/0606168 (2006).

1. Introduction

Besides the traditional telecom and datacom applications, silicon photonics is considered a promising technology for a much wider range of applications. One of these applications is spectroscopic sensing, which plays an important role in environmental monitoring, chemical process control, security and medical applications [1,2]. The sensitivity of a spectroscopic sensor can be significantly improved by operating in the mid-infrared wavelength region (3–12 μm wavelength) due to the orders of magnitude higher optical absorption cross-section in this range as compared to the telecom and visible wavelength range [3–6]. Due to high absorption of SiO_2 layer in mid-infrared [7], the SOI platform is limited to operation up to 3.8 μm [8]. Hence, multiple silicon-based platforms have been explored for the implementation of midIR photonic integrated circuits (PICs) beyond 3.8 μm , some of which rely on a suspended Si membrane [9], a silicon-on-sapphire layer stack [10] or graded index GeSi waveguides [11]. While bulk Si is considered transparent only up to a wavelength of 8 μm , Ge has low losses in the 2–14 μm wavelength range [7], which - together with its compatibility with standard CMOS/MEMS processes - makes it suitable for the implementation of midIR PICs. Recently, Ge-on-Si and Ge-on-silicon-on-insulator (Ge-on-SOI) have emerged as platforms for sensing applications beyond a wavelength of 4 μm [12–15]. The Ge-on-Si platform benefits from a simple fabrication

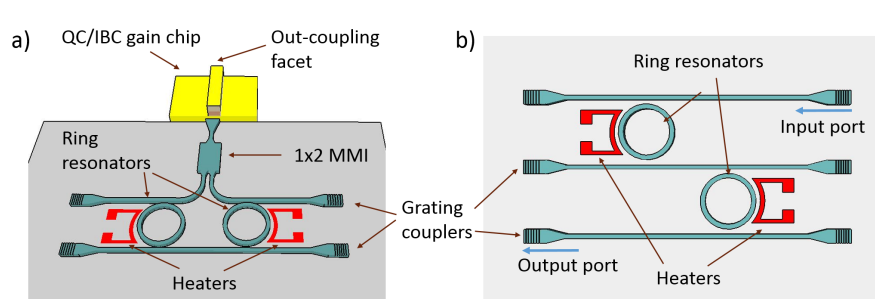


Fig. 1. A widely tunable external cavity QCL/ICL without any moving parts: the rotating grating is replaced by a tunable reflector on a chip. The tunable filter consists of a beam combiner/splitter and a Vernier ring resonator in a loop configuration (a), a tunable Vernier filter based on racetrack resonators that was used in the experiment (b).

process and should provide a wider transparency window compared to the other silicon-based mid-IR platforms. Unlike the Ge-on-Si platform, the Ge-on-SOI stack has an additional SiO₂ layer, which allows for more efficient integrated thermo-optic phase shifters [16]. The Si device layer in the SOI substrate of the Ge-on-SOI platform is thick enough to prevent overlap of the Ge waveguide mode with the underlying oxide, hence the mode does not incur losses from the highly absorptive oxide at 5 μm wavelength. The fabrication of devices on this platform can also take advantage of the additional SiO₂ layer to under-etch parts of the PIC, such as to further improve the efficiency of thermo-optic phase shifters and diffractive grating couplers [17].

An interesting implementation of widely tunable mid-IR lasers on this Ge-on-SOI platform is to butt couple a midIR III-V gain chip to the silicon photonic IC that comprises a widely tunable filter for the laser wavelength selection. Gain materials of interest in the mid-infrared are quantum cascade (QC) structures [18] and interband cascade (IBC) structures [19]. Broadband gain quantum cascade lasers (QCLs) have been demonstrated with watt-level output power operating at room temperature in the mid-infrared region [20], while lower-power-consumption interband cascade laser (ICL) structures are emerging as well [21]. Wavelength tuning however currently relies mostly on incorporating an external grating which provides feedback to the laser and defines its emission wavelength. Tuning by rotating the external gratings depends on a highly precise rotation mechanism that is prone to instabilities. The implementation of a MEMS-based tunable diffraction grating partly overcomes these issues [22], however the assembly process remains cumbersome. To avoid these issues we can implement the external cavity on a chip aiming to replace the external rotating grating. One of the gain chip/PIC designs that can be used for this purpose is shown in Fig. 1(a). The QC or IBC gain chip has an outcoupling facet on the far end of the cavity, while the other reflector consists of a thermally tunable Ge-on-SOI integrated reflector for wavelength selection. The integrated reflector consists of a beam splitter/combiner such as a 1x2 multimode interferometer [16] and a Vernier racetrack resonator filter in a loop configuration. In this paper we demonstrate the operation of a tunable Vernier racetrack resonator circuit implemented on the Ge-on-SOI platform. We focus our work on the 5.25-5.4 μm wavelength range. In this wavelength region we can find absorption lines of acetylene, formic acid, ammonia and many other compounds of interest [23].

2. Design and simulations

In Fig. 1(b) we show the device structure under study used to validate the functionality of the tunable Vernier filter on the Ge-on-SOI platform in the 5 μm wavelength range. Two racetrack resonators are implemented on the Ge-on-SOI waveguide platform with a 2 μm thick germanium waveguide layer on a 3.2 μm silicon bottom cladding and a 2 μm thick SiO₂ layer. Heaters are implemented on the side of the Ge waveguide. Fiber-to-chip grating couplers are used to interface to the photonic integrated circuit.

The racetrack resonators have a transmission to the through port T_p and the drop port T_d given by [24]:

$$T_p = \frac{t^2 a^2 - 2t^2 a \cos \phi + t^2}{1 - 2t^2 a \cos \phi + t^4 a^2} \quad (1)$$

$$T_d = \frac{(1 - t^2)^2 a}{1 - 2t^2 a \cos \phi + t^4 a^2} \quad (2)$$

where t is the self-coupling coefficient. It is related to the cross-coupling coefficient κ by $\kappa^2 + t^2 = 1$. a is the single-pass amplitude transmission of the racetrack resonator defined by $a = \sqrt{e^{-\alpha(2\pi r + 2L)}}$, where r and L are the racetrack radius and the coupler length and α is the power attenuation coefficient. $\phi = \beta(2\pi r + 2L)$ is the single-pass phase shift, with β being the

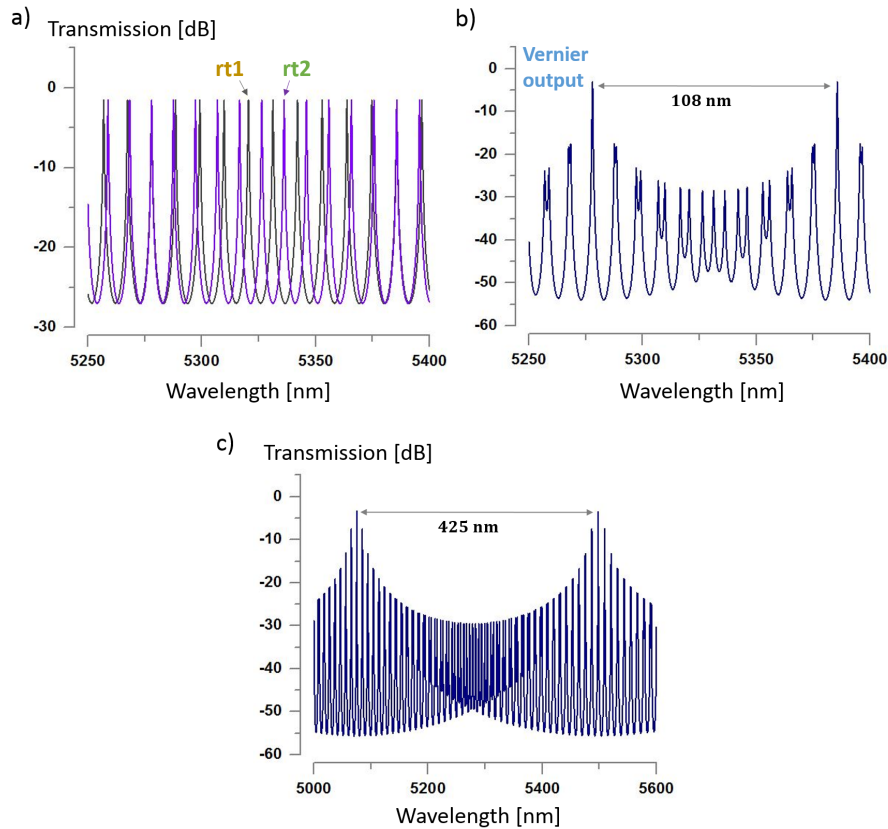


Fig. 2. The simulated transmission spectra T_d of individual racetrack resonators (a) and the transmission of the Vernier filter built with these racetracks (b). Simulation of a larger FSR_V Vernier filter (c).

propagation constant of the circulating mode. The racetrack resonator free spectral range (FSR) is determined by $FSR = \frac{\lambda^2}{n_g(2\pi r + 2L)}$, with n_g the group index.

FSR_V , the FSR of the Vernier filter, realized by cascading the individual resonators, depends on the individual FSRs of the racetrack resonators:

$$FSR_V = \frac{FSR_1 FSR_2}{FSR_1 - FSR_2} \quad (3)$$

The simulated T_d spectrum of individual rings with a radius of $100 \mu\text{m}$ and $110 \mu\text{m}$ are shown in Fig. 2(a), assuming a coupler length $L = 30 \mu\text{m}$, while in Fig. 2(b) the combined transmission of the Vernier filter is plotted. Here we assumed a group index $n_g = 4.2$, $t = 0.96$ and $a = 0.98$.

In this design, FSR_1 and FSR_2 are 9.7 nm and 8.9 nm respectively in the $5 \mu\text{m}$ wavelength range, leading to a combined FSR_V of 108 nm and the side-peak suppression is $>15 \text{ dB}$. The transmission of the Vernier filter reaches a maximum where the resonant peaks of the individual racetrack resonators overlap, which determines the lasing wavelength of the external cavity laser. By thermally adjusting the position of the overlapping transmission peaks the lasing wavelength can be tuned. The tuning range is limited by FSR_V . This free spectral range can be extended by reducing the difference in FSRs of the individual racetrack resonators. Using ring resonators with the same loaded Q-factor ($\sim 20,000$ in the example above), but with a radius of $100 \mu\text{m}$ and

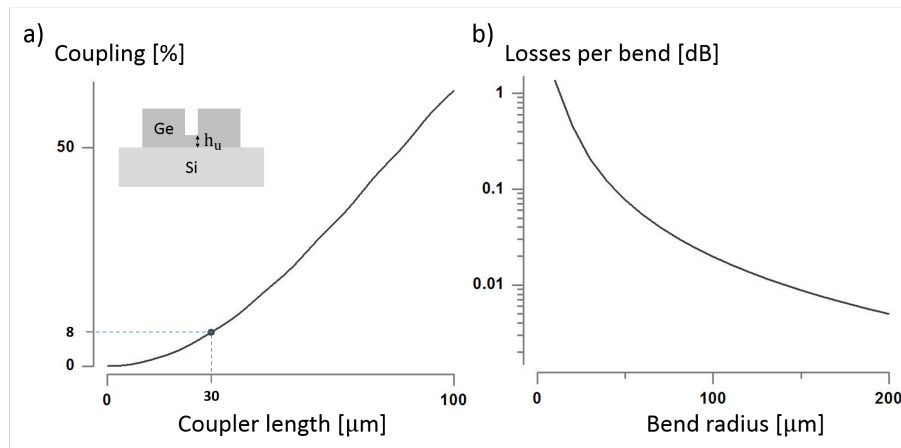


Fig. 3. Coupling to the racetrack resonator as a function of the coupler length (a) and the radiative losses per 90° bend (b).

$102.5 \mu\text{m}$ respectively, a combined free spectral range FSR_V of 425 nm can be obtained at the expense of a reduced side-peak suppression of 4 dB (Fig. 2(c)).

For the experiment discussed below, we have chosen to realize a Vernier racetrack resonator tunable filter based on resonators with a radius rt_1 and rt_2 of $100 \mu\text{m}$ and $110 \mu\text{m}$, respectively, while the length of the coupler L was chosen to be $30 \mu\text{m}$ in both resonators. This leads to an FSR of the individual resonators of 9.7 nm and 8.9 nm respectively, similar to the numerical example above. In this case the tunable filter could be characterized over an entire FSR_V of 108 nm with the available continuous wave QCL operating in the $5.25\text{-}5.4 \mu\text{m}$ wavelength range.

The Ge-on-SOI single mode waveguide structures were chosen to be $2.2 \mu\text{m}$ wide and fully etched through the $2 \mu\text{m}$ thick Ge waveguide layer, while the gap between the racetrack resonator and bus waveguide was chosen to be $0.5 \mu\text{m}$. The simulated power coupling efficiency as a

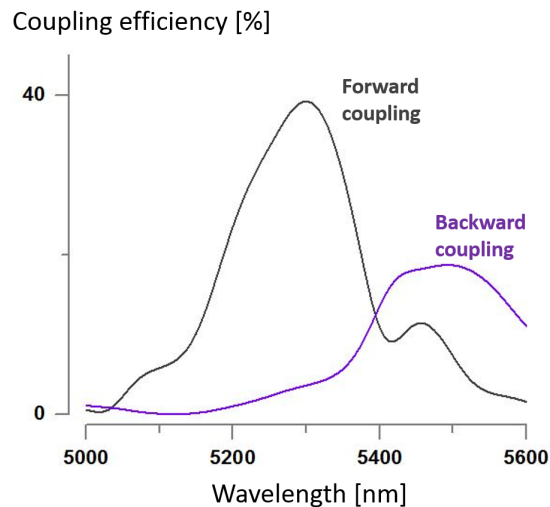


Fig. 4. The simulations of forward and backward coupling to the waveguide by the grating coupler.

function of coupler length (TM-polarization), calculated using a full-vectorial FDE tool is shown in Fig. 3(a). Due to etching process we used, Ge layer is not fully etched in the coupler region, leaving a slab of $h_u = 450$ nm. The simulated coupling efficiency for a coupler length of $0 \mu\text{m}$ is $< 0.1\%$, which indicates that the coupling in bends is negligible. This increases to 8% for a coupler length of $30 \mu\text{m}$. The bend radiation loss per 90 degree bend of the fully etched waveguide at a wavelength of $5.3 \mu\text{m}$ is shown in Fig. 3(b) as a function of bending radius.

The grating coupler structures used to characterize the PIC by interfacing with a single mode InF fiber [25] at $5.3 \mu\text{m}$ wavelength, are etched $1 \mu\text{m}$ deep, have a grating period of $1.45 \mu\text{m}$ and a grating duty cycle of 0.8 (duty cycle being the ratio of the width of the unetched part and the period). 30 periods were implemented to have a good coupling efficiency to the InF fiber with a mode field diameter of $18 \mu\text{m}$ [17]. The fiber is tilted 5 degrees off-normal. The simulated coupling spectrum in both forward and backward direction, when launching the fiber mode, is shown in Fig. 4. The small fiber angle causes some coupling of light in the backward direction, which in case of an abrupt termination of the waveguide causes back-reflections and interference. Therefore, in order to reduce the reflections, the waveguide in the backward direction is tapered down.

3. Device fabrication

A combination of electron-beam lithography and optical lithography is used to define the Ge-on-SOI waveguide circuit, comprising a $1 \mu\text{m}$ deep etch for the grating couplers and a $2 \mu\text{m}$ deep etch for the waveguide structures and racetrack resonators (Fig. 5).

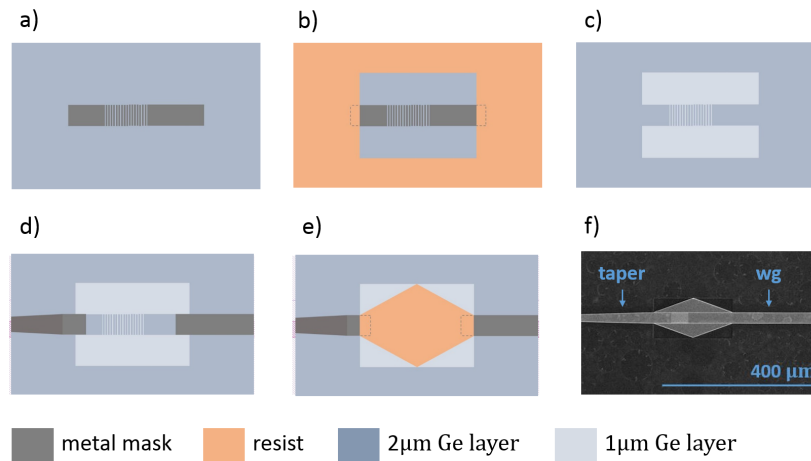


Fig. 5. Top view of the fabrication scheme for combining partially etched gratings and a fully etched waveguide circuit, by combining electron beam and optical lithography.

In the first step we use a positive e-beam resist (AR-P 6200.09) to define a Ti/Cr (5 nm and 50 nm thick respectively) metal mask through a lift-off process, for the partial etching of the gratings (Fig. 5(a)). Since we define only the gratings with positive e-beam resist, it is necessary to protect the rest of the sample (Fig. 5(b)), for which we use a photoresist (AZ9260). CF_4/H_2 reactive ion etching is then used to do the $1 \mu\text{m}$ deep partial etch (Fig. 5(c)). After etching, the remaining photoresist is removed using acetone and isopropylalcohol, after which the metal mask is removed using HF. A second e-beam lithography is then used to define the rest of the circuit, including the fully etched racetrack resonators (Fig. 5(d)). We use the same positive resist as in the first e-beam lithography to define a 5 nm Ti / 80 nm Cr hard mask through lift-off. The

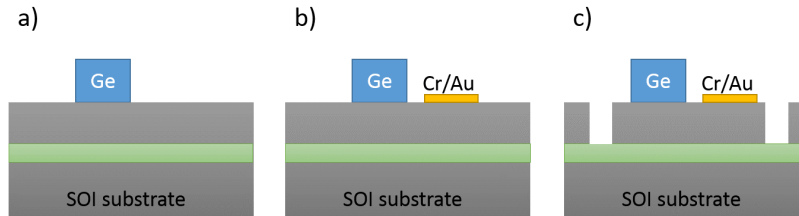


Fig. 6. The fabrication process for defining heaters for thermal tuning.

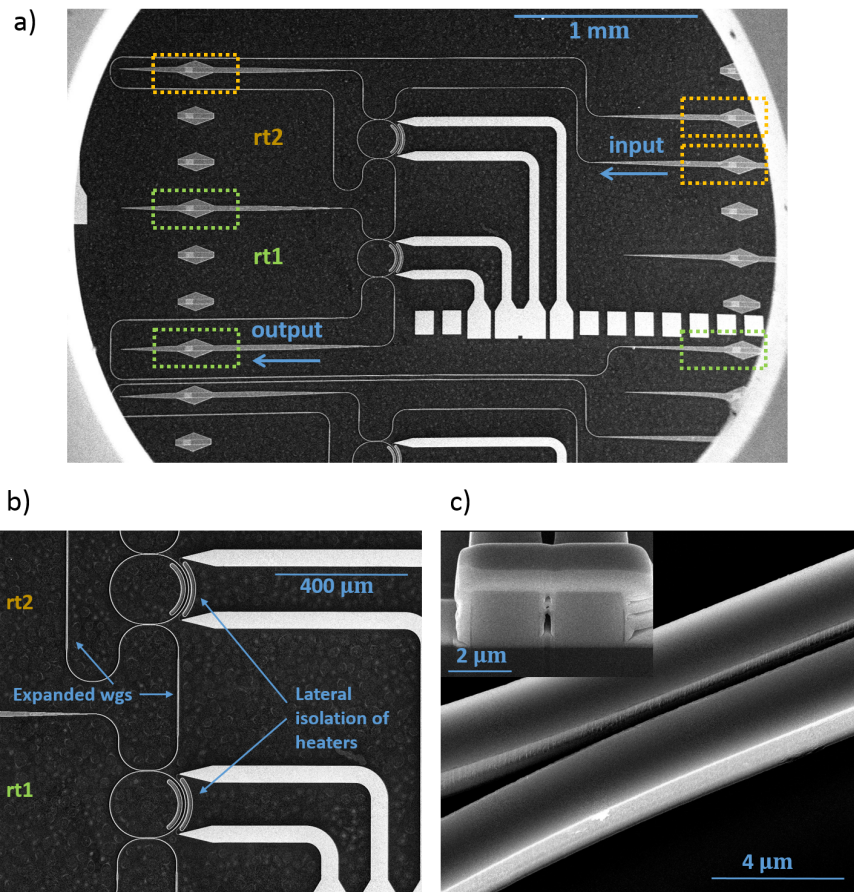


Fig. 7. The chip layout: the two racetrack resonators in a Vernier configuration with ports that allow to measure the response of each individual resonator (a, b). The coupling section of a racetrack with its cross-section in the straight part of the coupler (c). The cladding-like structure on the cross-section image is platinum that was deposited to protect the waveguides while making a focused ion beam cross-section of the waveguide.

coupler gap in the racetrack resonators is defined to be 450 nm wide, which broadens to 500 nm after the dry etching. The thickness of the e-beam resist for the second e-beam lithography is 400 nm, which is not enough to efficiently cover the 1 μm partially etched gratings. Therefore we

again use AZ9260 photoresist to protect the gratings (Fig. 5(e)).

The protective structures defined in the AZ9260 photoresist have a tapered shape such that there is a smooth transition from the grating to the fully etched waveguide. In order to reduce the influence of fabrication imperfections on the circuit performance we make sure that the two e-beam lithography patterns overlap on the slab section of the grating before tapering down to the single-mode waveguide. The second etching step is done in the same CF_4/H_2 plasma until the Ge-Si interface is reached (Fig. 5(f)), after which the photoresist and the metal mask are stripped resulting in the waveguide structure shown in Fig. 6(a). Next, Cr/Au heaters for the thermal tuning of the individual rings are defined with an image reversal lithography using Ti35 resist and lift-off. The Cr/Au (100 nm and 10 nm respectively) heaters are deposited by electron beam evaporation (Fig. 6(b)). The buried oxide layer in the SOI prevents efficient heat sinking into the Si substrate, which enhances the efficiency of the heaters. To better thermally isolate the heaters laterally and thereby improve their efficiency, we additionally etch through the top Si layer to reach the SiO_2 in the vicinity of the heaters (Fig. 6(c)). For this AZ9260 photoresist and a $\text{CHF}_3/\text{SF}_6/\text{O}_2$ plasma is used.

The e-beam write field is $500\ \mu\text{m}$ by $500\ \mu\text{m}$, which allows accommodating the racetracks in a single write field and hence avoid degradation of the Q-factor by stitching errors. On other places where we cannot avoid stitching, we are expanding the waveguides to a width of $5\ \mu\text{m}$ as they incur less losses when stitching errors occur. SEM images of the final device are shown in Fig. 7 starting with a general overview of the Vernier filter in 7(a), a zoom in on the racetrack resonators in 7(b) and a detailed view of the coupler section of the individual resonator in 7(c).

4. Measurements

4.1. Measurement setup

The measurement setup is schematically shown in Fig. 8. Light from the free-space emitting QCL operating in continuous wave is coupled to an InF single mode fiber. Between the laser and the fiber coupler we have a CaF_2 beam splitter, a Babinet-Soleil polarization control element and

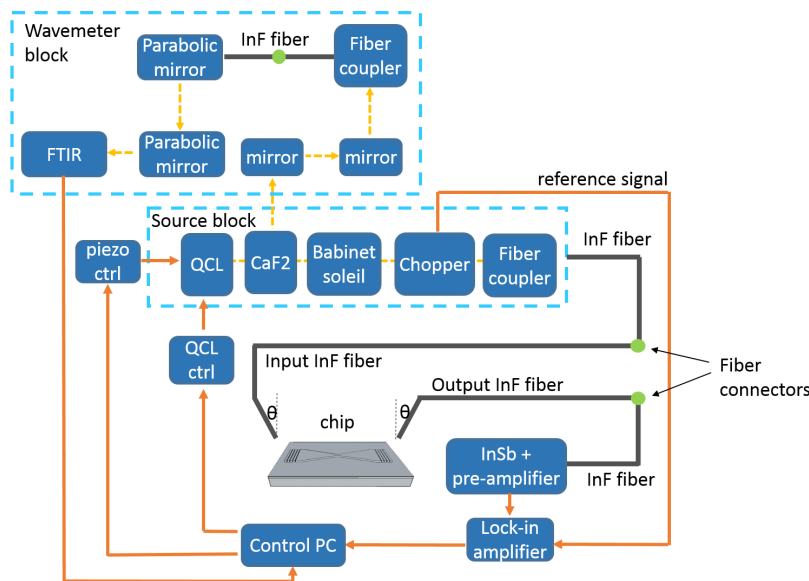


Fig. 8. The measurement setup.

a chopper. The chopper turns the CW light into 50% duty cycle pulses and hence allows us to detect the signal using a pre-amplified InSb detector and a lock-in amplifier. With the polarization control element the input polarization state is set to the TM polarization. The light reflected by the CaF₂ beam splitter is sent to an FTIR for precisely monitoring the laser wavelength.

All of our measurement results are reported relative to a reference waveguide consisting of two fiber-to-chip grating couplers. The single mode waveguide section on this reference structure is 20 μm long, which is short enough to neglect losses caused by the waveguiding.

4.2. Measurement results

The chip layout (Fig. 7(a)) allows us to test the racetrack resonators used to build the Vernier filter individually - using the grating coupler ports marked in green in case of racetrack 1 ($r_{t1} = 100 \mu\text{m}$) and the grating coupler ports marked with orange squares for racetrack 2 ($r_{t2} = 110 \mu\text{m}$), as well as the complete Vernier filter.

The measured transmission of the through and drop ports of the individual racetrack resonators are shown in Fig. 9(a), showing a loaded Q-factor of 18000 and 19000 respectively. The measured

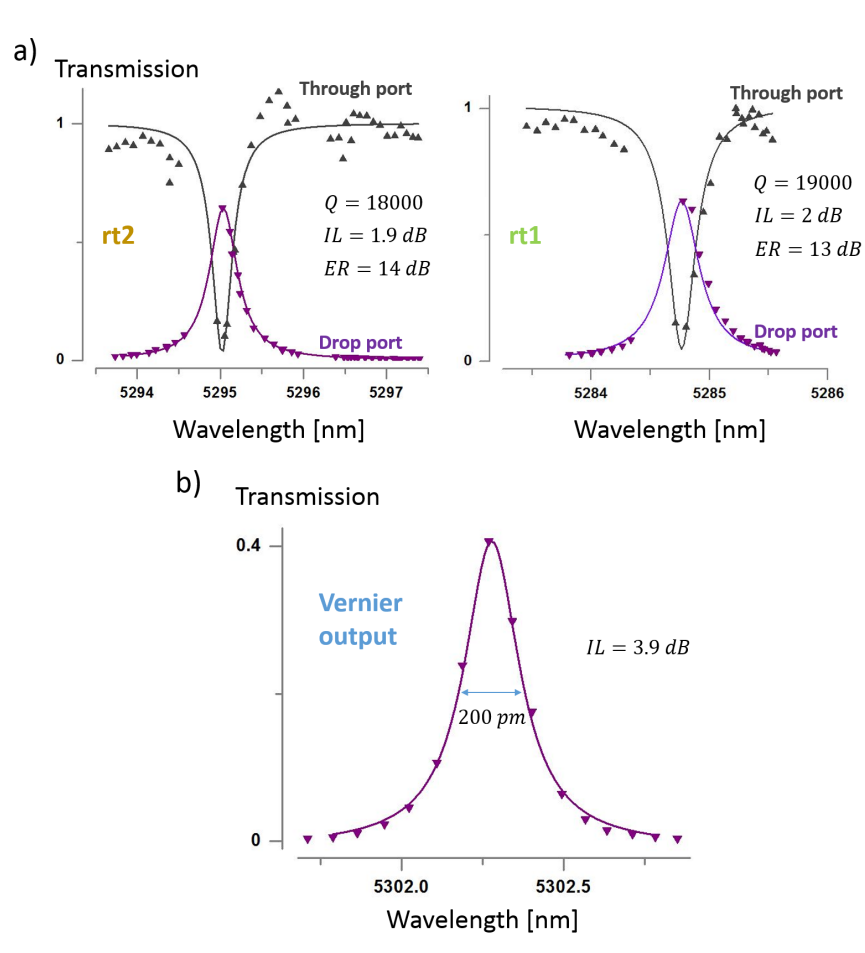


Fig. 9. Measured and fitted transmission of through and drop port of the individual racetrack resonators when not heated (a), and of the Vernier filter when aligned by heating one of the racetracks (b).

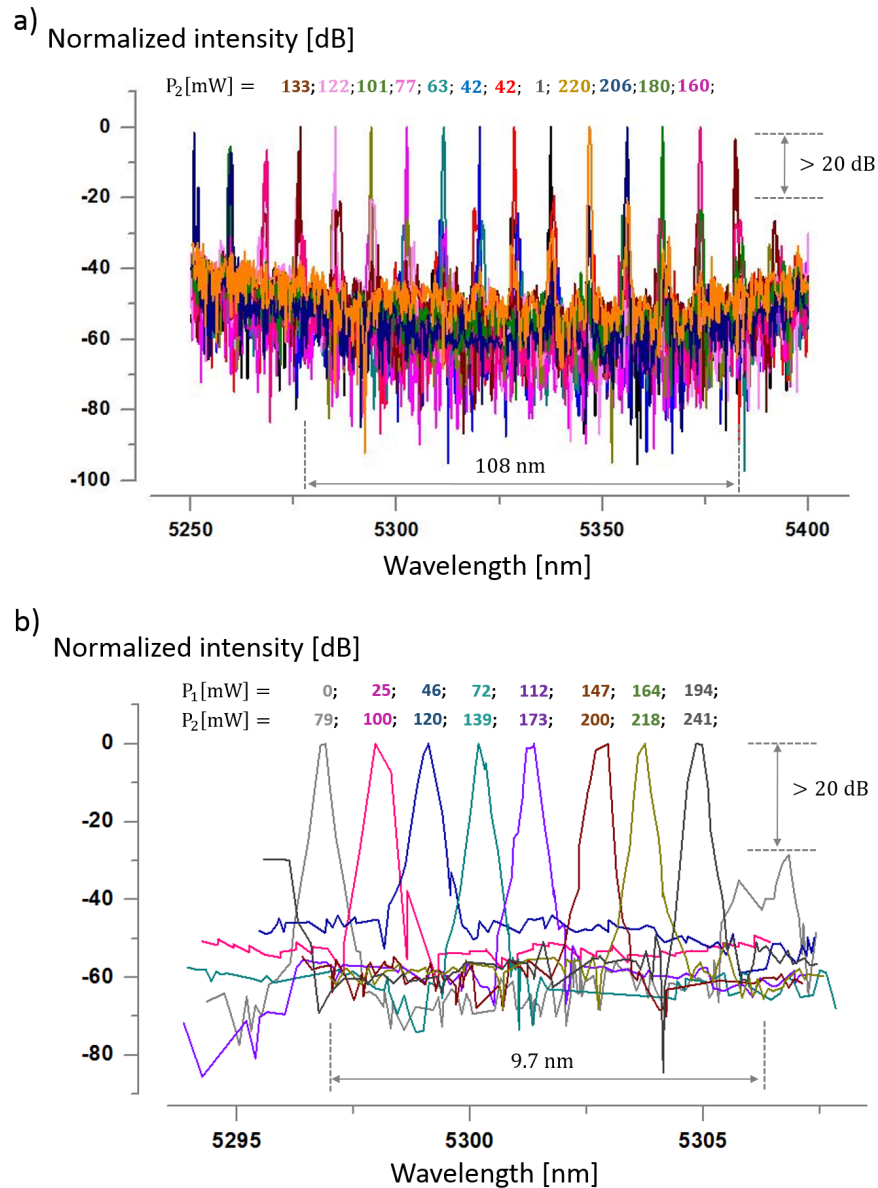


Fig. 10. The discrete tuning of the Vernier filter. By thermally tuning resonator 2, one can tune the resonant wavelength of the filter in steps of the FSRs of the resonator1 that is not tuned (a). The fine tuning of the Vernier filter by tuning both racetrack resonators together such that we have maximum transmission at the wavelength of choice. Here we show the fine tuning for a few wavelengths with a step of approximately $2FWHM$ over the FSR of the individual racetrack (b).

extinction ratio (ER) is 14 dB and 13 dB, respectively, while the insertion loss (IL) is 1.9 dB and 2 dB. The full width at half maximum (FWHM) of the Vernier filter for a case where the resonance wavelengths of both racetrack resonators are aligned is 200 pm, while the IL is 3.9 dB.

For $r = 100\mu\text{m}$ and $L = 30\mu\text{m}$, the parameters we get from the fitting of the racetrack resonator

spectra are $t = 0.96$ and $a = 0.98$ corresponding to waveguide loss of 2.5 dB/cm. An FSR_V of 108 nm is experimentally obtained.

By thermally tuning one of the racetrack resonators the position of the overlapping transmission peak can be tuned in steps of the FSR of the other resonator. This way, discrete tuning of the filter can be realized as shown in Fig. 10(a). Accessing wavelengths in between resonances of the resonator that was not tuned, can be achieved by tuning both racetrack resonators at the same time. This is illustrated in Fig. 10(b). To access any arbitrary wavelength within the FSR_V of the Vernier filter the total power dissipation of the filter is less than 500mW. The side-peak suppression of the filter transmission is more than 20 dB.

In order to assess the temperature dependence of the filter, transmission spectra of racetrack 2 were characterized at different stage temperatures. The resonant wavelength shift as a function of stage temperature, given by

$$\Delta\lambda = \frac{dn}{dT} \frac{\lambda}{n_g} \Delta T \quad (4)$$

is shown in Fig. 11(a).

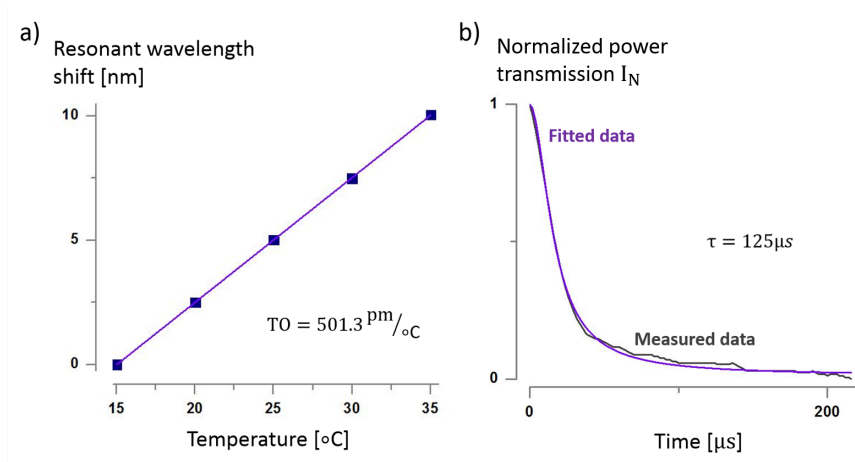


Fig. 11. The resonant wavelength shift as a function of ambient temperature (a). Measurement data and fitting of the tuning speed of the resonator (b).

A thermo-optic coefficient of $501.3 \pm 12.5 \frac{pm}{°C}$ is measured, which is close to the calculated value of $520 \frac{pm}{°C}$, using the Ge thermo-optic coefficient of $\frac{dn}{dT} = 4.2 \times 10^{-4} K^{-1}$ at $5.2 \mu m$ wavelength [26].

The racetrack resonator response time to a step in the heater voltage is shown in Fig. 11(b). For this experiment the laser wavelength was aligned with a resonance of the ring resonator, after which a step function in the heater current was applied which detunes the resonance from the laser wavelength and results in a drop in transmission at the drop port. Assuming a first order response of the resonator detuning and taking into account the Lorentzian line shape of the resonance with a full width at half maximum $FWHM$, we have:

$$I_N = \frac{1}{1 + \left(\frac{2 \cdot \Delta\lambda \cdot (1 - e^{-t/\tau})}{FWHM}\right)^2} \quad (5)$$

where I_N is the normalized power transmission, $\Delta\lambda$ is the steady state change in the resonator wavelength from an ON-resonance state to an OFF-resonance state and τ is the time constant. $\Delta\lambda$

is obtained by comparing the applied step in the heater power dissipation with the power needed to tune over the *FSR* of of the resonator. By fitting, we get the time constant of 125 μ s.

5. Conclusion

We have fabricated thermally tunable racetrack resonators with a Q-factor of \sim 20000 and a free spectral range of \sim 9 nm on the Ge-on-SOI platform, operating in the 5 μ m wavelength range. With these resonators we demonstrate a tunable Vernier filter with a free spectral range of 110 nm and a side-peak suppression $>$ 20 dB. The power needed to continuously tune over the full *FSR* of the Vernier filter is 500 mW combined power of the two heaters. Our simulations show that using the racetrack resonators with a Q-factor of 20000 we can enlarge the free spectral range of the Vernier filter up to 425 nm and still maintain a 4 dB side-peak suppression. The temperature dependence of the filter characteristic was assessed, resulting in a resonant wavelength shift of 0.5 nm/K. The response time of the thermally tunable racetrack resonator was measured to be 125 μ s, allowing for kHz rate wavelength tuning.